
DIRECTED GRAPH AUTO-ENCODERS

Georgios Kollias, Vasileios Kalantzis, Tsuyoshi Idé, Aurélie Lozano, Naoki Abe
IBM Research
T. J. Watson Research Center
{gkollias, vkal, tide, aclozano, nabe}@us.ibm.com

ABSTRACT

We introduce a new class of auto-encoders for directed graphs, motivated by a direct extension of the Weisfeiler-Leman algorithm to pairs of node labels. The proposed model learns pairs of interpretable latent representations for the nodes of directed graphs, and uses parameterized graph convolutional network (GCN) layers for its encoder and an asymmetric inner product decoder. Parameters in the encoder control the weighting of representations exchanged between neighboring nodes. We demonstrate the ability of the proposed model to learn meaningful latent embeddings and achieve superior performance on the directed link prediction task on several popular network datasets.

Introduction

Graph-structured data are ubiquitous, commonly encountered in diverse domains, ranging from biochemical interaction networks, to networks of social and economic transactions. A graph introduces dependencies between its connected nodes, thus algorithms designed to work solely with feature vectors of isolated nodes as inputs can yield suboptimal results. One way to remedy this issue, without reverting to more complex graph algorithms, is to enhance the representation of a graph node so that both its features and embedding graph structure are captured in a single vector.

Graph Convolutional Networks (GCNs) produce vectorial representations of nodes that are graph-aware and have been successfully used in downstream learning tasks including node classification, link prediction and graph classification. The construction of GCNs falls into two categories: spatial-based and spectral-based. Spatial-based GCNs are conveniently described as Message Passing Neural Networks (MPNNs) detailing the steps for aggregating information from neighbor graph nodes Gilmer et al. (2017); Micheli (2009); Niepert et al. (2016). They adopt a local view of the graph structure around each node and are straightforward to describe and lightweight to compute; however they also need local customizations to enhance the performance of the representations they produce for downstream learning tasks Veličković et al. (2017). Spectral-based GCNs originate in graph signal processing perspectives Bruna et al. (2014). They are based on the graph Laplacian, so they inherently adopt a global graph view Defferrard et al. (2016); Kipf and Welling (2016a). However they incur more computational cost, typically addressed by approximating their convolutional filter.

In this work we focus on GCN-based models for representing the nodes of directed graphs (encoding), so that we can faithfully reconstruct their directed edges (decoding). Our goal is to identify both whether two nodes u and v should be connected or not (which is the only goal for the undirected case) and whether their connection has the direction $u \mapsto v$ or $v \mapsto u$ or both. Many applications depend critically on this distinctuality. For example in (directed) citation graphs it cannot be the case that a publication cites a work that is published later in time, in (directed) causal graphs a causal node should prehend any of its effects, in knowledge graphs subject nodes are expected to point to object nodes. As a consequence, failing to identify the correct orientation even in a single edge could severely disrupt downstream tasks: time ordering can become contradicting, paths to root causes can be erroneously blocked, flow computations between entities can be totally wrong.

Our encoder follows a color refinement scheme for directed graphs that reduces to the standard Weisfeiler-Leman algorithm. Coupled with an unsymmetric decoder, our directed graph auto-encoder can accurately infer missing directed links from the limited, incomplete graph it has access to during training time.

Our contributions are two-fold. First, we propose a novel variant of the Weisfeiler-Leman algorithm that clearly emphasizes the dual role of directed graph nodes as both sources and targets of directed links. This abstracts, for the first time, the alternating update of authority and hub scalar values in HITS, and the relations between left and right singular vectors computed in SVD and the GCN-based approaches for directed graphs inspired by them. Second, we design parameterized GCN layers for updating the pair-of-vectors representation of the source and target roles of directed graph nodes in an alternating manner, and use these layers as the encoder in a directed graph auto-encoder architecture. We demonstrate that the parameterization we introduce is performance-critical for learning latent representations, and the proposed model can outperform state-of-the-art methods for the *directed* link prediction task on several popular citation network datasets in terms of area under the ROC curve (AUC) and average precision (AP) metrics.

The code is available at <https://github.com/gidiko/DiGAE>.

Preliminaries and background

We can generally describe the dependencies of a network as a directed graph $G(V, E, w)$, i.e., a weighted *dependency graph*. Here V is the set of $n = |V|$ graph nodes and $E = \{(i, j) \in V \times V : i \mapsto j\}$ is the set of its $m = |E|$ directed edges, expressed as node pairs. Finally $w : V \times V \rightarrow \mathbb{R}$ is the edge weight function, with $w(i, j)$ being a scalar capturing the “strength” of the dependency $i \mapsto j$ iff $(i, j) \in E$ - and vanishing otherwise. Following a linear algebra perspective, we will represent $G(V, E, w)$ as an $n \times n$ sparse, weighted, adjacency matrix \mathbf{A} . This matrix has m non-vanishing entries and its (i, j) entry is set equal to the respective weight $w(i, j)$, i.e., $\mathbf{A}[i, j] = w(i, j)$. Throughout the rest of this paper, we use $\tilde{\mathcal{N}}^+(i) = \mathcal{N}^+(i) \cup \{i\}$ ($\tilde{\mathcal{N}}^-(i) = \mathcal{N}^-(i) \cup \{i\}$) and $\text{deg}^+(i) = |\tilde{\mathcal{N}}^+(i)|$ ($\text{deg}^-(i) = |\tilde{\mathcal{N}}^-(i)|$), to denote the neighbor node sets of the outgoing (incoming) edges and outgoing (incoming) degrees of a node i - including itself. Analogously, the corresponding diagonal matrices with the outdegrees (indegrees) along their diagonal will be denoted as $\tilde{\mathbf{D}}^+$ ($\tilde{\mathbf{D}}^-$), where we top with a tilde mark the names of adjacency matrices with added self-links. Note that for undirected, unweighted graphs, the corresponding adjacency matrices are symmetric and binary, i.e., $\tilde{\mathbf{D}}$ is a diagonal matrix where \tilde{d}_{ii} is the original degree of node i increased by 1 (because of the added self-link).

Dual vector encoding of directed graph nodes

Consider a directed edge $i \mapsto j$, with weight $w(i, j)$, where i is the source node and j is the target node. Now, let’s assume that node i is equipped with a pair of vectors in \mathbb{R}^k , $1 \leq i \leq n$: (i) vector \mathbf{s}_i encodes i ’s role as a source, which is the same for any of the directed edges it participates as a source, and (ii) vector \mathbf{t}_i encodes i ’s role as a target; similarly for node j . The similarity of nodes i and j in building the weighted directed edge $i \mapsto j$ could then be captured by a similarity function $\text{sim}(\cdot, \cdot)$ which ideally evaluates to the true edge weight: $\text{sim}(\mathbf{s}_i, \mathbf{t}_j) = w(i, j)$.

An immediate choice for the similarity function is the dot product: $\text{sim}(\mathbf{s}_i, \mathbf{t}_j) = \mathbf{s}_i^\top \mathbf{t}_j$, with the encodings originally realized as column vectors. We then can compactly evaluate the weights of all edges, by building two matrices, \mathbf{S} and \mathbf{T} , where $\mathbf{S}[i, :] = \mathbf{s}_i^\top$ and $\mathbf{T}[j, :] = \mathbf{t}_j^\top$, for all $1 \leq i, j \leq n$, and requiring $\mathbf{A} = \mathbf{S}\mathbf{T}^\top$. This particular choice has been explored in Ou et al. (2016), which leverages the singular value decomposition (SVD) $\mathbf{A} = \mathbf{U}\Sigma\mathbf{V}^\top$ and sets $\mathbf{S} = \mathbf{U}\Sigma^{\frac{1}{2}}$ and $\mathbf{T} = \mathbf{V}\Sigma^{\frac{1}{2}}$. The authors also explore a variant based on truncated SVD.

Weisfeiler-Leman (WL) algorithm and connection to GCNs

One-dimensional Weisfeiler-Leman (1-WL)

One dimensional Weisfeiler-Leman (1-WL) algorithm is a well-studied approach for assigning distinct labels to the nodes of undirected, unweighted graphs with different topological roles Weisfeiler and Leman (1968). Given adjacency information in the form of neighborhood lists $\mathcal{N}(i) = [k : i \mapsto k \vee k \mapsto i]$, $\forall i \in [0, n)$, 1-dim WL iteratively updates a node’s label by computing a bijective hash of its neighbors’ labels, and mapping this to a unique label. The procedure terminates when the hash-and-map procedure stabilizes. A detailed sketch of the 1-WL algorithm is provided in the Appendix.

Graph Convolutional Network (GCN)

Graph Convolutional Networks (GCNs) suggest convolution operators for graph signals defined over graph nodes. Following the early analysis in Hammond et al. (2011) and the expansions in Defferrard et al. (2016), GCNs were particularly popularized by Kipf et al. Kipf and Welling (2016a). In particular, the work in Kipf and Welling (2016a)

focused on undirected, unweighted graphs, such that the adjacency matrices are symmetric and binary. Each node i is initially assumed encoded by a $k = k_0$ dimensional vector \mathbf{x}_i , so all node encodings can be collected in an $n \times k$ matrix $\mathbf{X} = \mathbf{X}^{(0)}$. The goal is to *transform* the node embeddings so that a downstream task such as node classification is more accurate.

The proposed transformation contains a succession of *graph convolutional layers* of the form:

$$\mathbf{Z}^{(t)} \leftarrow \tilde{\mathbf{D}}^{-\frac{1}{2}} \tilde{\mathbf{A}} \tilde{\mathbf{D}}^{-\frac{1}{2}} \mathbf{X}^{(t)} \mathbf{W}^{(t)} \quad (1)$$

interspersed with *nonlinear layers*, like ReLU and softmax. The quantity $\mathbf{W}^{(t)}$ is a *learnable* $k_t \times k_{t+1}$ matrix of weights for the t^{th} *graph convolutional layer* ($t = 0, 1, \dots$). The algorithm in Kipf and Welling (2016a) implements the transformation of the original encodings \mathbf{X} :

$$\mathbf{Z} \leftarrow \text{softmax}(\hat{\mathbf{A}} \text{ReLU}(\hat{\mathbf{A}} \mathbf{X} \mathbf{W}^{(0)}) \mathbf{W}^{(1)}), \quad (2)$$

where $\hat{\mathbf{A}} := \tilde{\mathbf{D}}^{-\frac{1}{2}} \tilde{\mathbf{A}} \tilde{\mathbf{D}}^{-\frac{1}{2}}$.

Connecting 1-WL to GCNs

In Morris et al. (2019) the connection of 1-WL to 1-GNNs is explored. Their basic 1-GNN model assumes the form

$$f^{(t)}(v) = \sigma \left(f^{(t-1)}(v) \cdot W_1^{(t)} + \sum_{w \in N(v)} f^{(t-1)}(w) \cdot W_2^{(t)} \right) \quad (3)$$

In this, $f^{(t)}(v)$, which is the row feature vector of node v at layer $t > 0$, is computed by aggregating its feature vector and the feature vectors of its neighbors at the previous layer $t - 1$, after first multiplying them respectively by parameter matrices $W_1^{(t)}$ and $W_2^{(t)}$. It follows GCNs are 1-GNNs. These results establish the connection of 1-WL to 1-GNNs (3):

- **[Theorem 1 in Morris et al. (2019)]** For all $t \geq 0$ and for all choices of weights $\mathbf{W}^{(t)} = (W_1^{(t)}, W_2^{(t)})_{t' \leq t}$, coloring $c_l^{(t)}$ refines encoding $f^{(t)}$: $c_l^{(t)} \sqsubseteq f^{(t)}$. This means that for any nodes u, w in G_{st} , $c_l^{(t)}(u) = c_l^{(t)}(w)$ implies $f^{(t)}(u) = f^{(t)}(w)$.
- **[Theorem 2 in Morris et al. (2019)]** For all $t \geq 0$ there exists a sequence of $\mathbf{W}^{(t)}$ and a 1-GNN architecture such that the colorings and the encodings are equivalent: $c_l^{(t)} \equiv f^{(t)}$ (i.e. $c_l^{(t)} \sqsubseteq f^{(t)}$ and $f^{(t)} \sqsubseteq c_l^{(t)}$).

DiGAE: Directed Graph Auto-Encoder

Weisfeiler-Leman (WL) algorithm and connection to encoder layers in DiGAE

We now extend 1-WL for coloring pairs of node labels in directed graphs. We can formally prove that this extension reduces to standard 1-WL over a bipartite, undirected graph. This allows us to connect it to 1-GNNs with a special structure for the parameter matrices, which corresponds to the directed graph convolutional layers in the encoder module of our DiGAE architecture which we define next. For the case of shared weight matrices we can even remove this special structure requirement.

Coloring pairs of node labels in directed graphs

To extend 1-WL for directed graphs, we equip each node of the graph with 2 labels, one for capturing its role as a “source” of directed edges emanating from it and another one for its role as a “target” node for directed edges pointing to it. Then at each step, we propose the “source” label of a node to be a bijective function of its current “source” label and the multiset of “target” labels of the nodes it points to. In parallel, its “target” label will be updated to the bijective mapping of its current target label and the “source” labels of the nodes pointing to it. For the detailed algorithm, please refer to the Appendix.

Neural Source and Target encodings

The propagation of “source” and “target” node labels along their directed edges, as in the extension of the 1-WL algorithm, suggests a new graph convolutional network layer. Similarly to the way the GCN layer is closely connected

to standard 1-WL, we propose a novel *directed graph convolutional layer* that transforms a pair of source and target encoding vectors for each node, in analogy to our extension for directed graphs. We assume that each node i is originally encoded by a pair of vectors, its *source* $\mathbf{s}_i^{(0)}$ and *target* $\mathbf{t}_i^{(0)}$ encodings, and collect these encodings as rows in matrices $\mathbf{S}^{(0)}$ and $\mathbf{T}^{(0)}$.

We can now define the t^{th} graph convolutional layer for updating the *source* encodings by aggregating the transformed and normalized *target* encodings in the neighborhood as:

$$\mathbf{S}^{(t+1)} \leftarrow \left(\tilde{\mathbf{D}}^+ \right)^{-\beta} \tilde{\mathbf{A}} \left(\tilde{\mathbf{D}}^- \right)^{-\alpha} \mathbf{T}^{(t)} \mathbf{W}_T^{(t)} \quad (4)$$

In this work we propose tunable parameters α and β for weighting the degrees in message passing. This subtle modification can have important effects in performance for the link prediction task as demonstrated in the experimental section.

Similarly we update the *target* encodings by aggregating the transformed and normalized *source* encodings in the neighborhood:

$$\mathbf{T}^{(t+1)} \leftarrow \left(\tilde{\mathbf{D}}^- \right)^{-\alpha} \tilde{\mathbf{A}}^\top \left(\tilde{\mathbf{D}}^+ \right)^{-\beta} \mathbf{S}^{(t)} \mathbf{W}_S^{(t)} \quad (5)$$

where $\mathbf{W}_T^{(t)}$ and $\mathbf{W}_S^{(t)}$ are the (learnable) linear transformations for target and encoding encodings prior to their propagation. Defining $\hat{\mathbf{A}} = \left(\tilde{\mathbf{D}}^+ \right)^{-\beta} \tilde{\mathbf{A}} \left(\tilde{\mathbf{D}}^- \right)^{-\alpha}$, we can compactly express our proposed graph convolutional layer by the following pair of transformations:

$$\begin{aligned} \mathbf{S}^{(t+1)} &\leftarrow \hat{\mathbf{A}} \mathbf{T}^{(t)} \mathbf{W}_T^{(t)} \\ \mathbf{T}^{(t+1)} &\leftarrow \hat{\mathbf{A}}^\top \mathbf{S}^{(t)} \mathbf{W}_S^{(t)}. \end{aligned} \quad (6)$$

Reduction to 1-WL

We consider the transformation of our directed, unweighted graph $G(V, E)$ to its *bipartite representation* $G_{st}(V_s, V_t, E_{st})$ with $V_s = V = [0, n)$, $V_t = [n, 2n)$ and $E_{st} = \{\{i, j+n\} | (i, j) \in E\}$ Bang-Jensen and Gutin (2008). The bipartite graph G_{st} is assumed undirected and it follows that for the set $\mathcal{N}_{st}(v)$ of the immediate neighbors of any of its nodes $v \in V(G_{st}) = V_s \cup V_t$:

$$\mathcal{N}_{st}(v) = \begin{cases} \{j+n | (v, j) \in E\} & \text{if } 0 \leq v < n \\ \{i | (i, v-n) \in E\} & \text{if } n \leq v < 2n \end{cases} \quad (7)$$

We also assume that the $2n$ nodes of G_{st} are initially colored with two colors in the set $\{s, t\}$ according to a coloring function $l : V_s \cup V_t \rightarrow \Sigma$ with $l(v) = s$, if $0 \leq v < n$ and $l(v) = t$, if $n \leq v < 2n$. In other words (G_{st}, l) is a labeled graph, so we can directly apply the standard 1-WL iterative algorithm for color refinement. In each iteration $t \geq 0$, 1-WL computes a node coloring $c_l^{(t)} : V(G_{st}) \rightarrow \Sigma$ with an arbitrary codomain of colors Σ . We initialize this sequence of colorings as $c_l^{(0)} = l$ and at $t > 0$, node coloring is updated as:

$$c_l^{(t)}(v) = \text{HASH} \left((c_l^{(t-1)}(v), \{\{c_l^{(t-1)}(w) | w \in \mathcal{N}_{st}(v)\}\}) \right)$$

Termination of this standard 1-WL algorithm is guaranteed after at most $|V(G_{st})| = 2n$ iterations and reached when $|c_l^{(t)}| = |c_l^{(t-1)}|$ for some k .

Essentially, the bipartite representation maps a node $i \in V$ in the directed graph G to a pair of nodes $(i \in V_s, i+n \in V_t)$ in the undirected, bipartite graph G_{st} : $i \in V_s$ represents $i \in V$ as a *source* of directed edges in G and $i+n \in V_t$ represents $i \in V$ as a *target* of directed edges in G . In addition, identical color pair labels (s, t) , initially assigned to all nodes $i \in V$ (in the directed graph G) are mapped to: (i) an initial label s for node $i \in V_s$ and (ii) an initial label t for node $i+n \in V_t$ (in the undirected, bipartite graph G_{st}). So in our refinement scheme for a node i in G , it holds $(c_{i,s}^{(0)}(i), c_{i,t}^{(0)}(i)) = (s, t)$ while for its corresponding nodes $i, i+n$ in G_{st} , $c_l^{(0)}(i) = s$ and $c_l^{(0)}(i+n) = t$.

We can now prove that the color pairs computed at each step k and for each node i by our refinement scheme on a directed graph G can equivalently be computed by standard 1-WL on the undirected, bipartite G_{st} by pairing the colors of its nodes i and $i+n$. In other words:

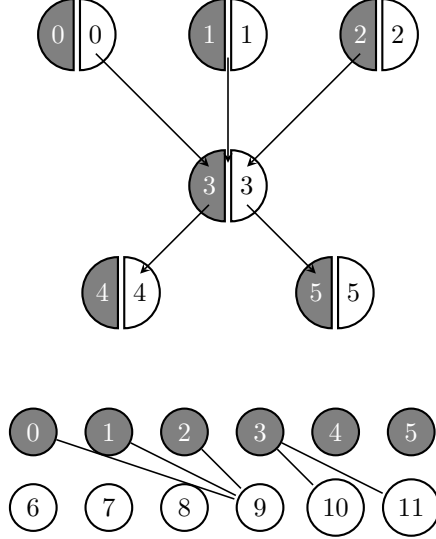


Figure 1: An example directed graph G with $n = 6$ nodes (top) and its bipartite representation G_{st} (bottom). Both graphs are colored with each node in G carrying a pair of source and target colors - respectively in left and right semidisks. The example node 3 in G maps to nodes 3 and 9 in G_{st} .

Theorem 1.

$$c_{l,s}^{(t)}(i) = c_l^{(t)}(i), c_{l,t}^{(t)}(i) = c_l^{(t)}(i + n) \quad (8)$$

for all layers $t \geq 0$ and $i \in [0, n)$.

Proof. We use induction. For $t = 0$ this holds by our initialization convention: $c_{l,s}^{(0)}(i) = c_l^{(0)}(i) = s$ and $c_{l,t}^{(0)}(i) = c_l^{(0)}(i + n) = t$.

Let us now assume that this also holds for some t and find out for $t + 1$. Consider a node with index $i \in [0, n)$. Its neighbors $w = j + n \in \mathcal{N}_{st}(i)$ in G_{st} map to the outlink-neighbors $j \in \mathcal{N}^+(i)$ in G according to our bipartite representation (see Equation (7)). These neighbors $w = j + n \in \mathcal{N}_{st}(i)$ have color labels $c_l^{(t)}(j + n)$ which according to (8) are equal to $c_{l,t}^{(t)}(i)$:

$$\begin{aligned} c_l^{(t+1)}(i) &= \text{HASH}((c_l^{(t)}(i), \{\{c_l^{(t)}(w) | w \in \mathcal{N}_{st}(i)\}\})) = \\ &= \text{HASH}((c_{l,s}^{(t)}(i), \{\{c_{l,t}^{(t)}(j) | j \in \mathcal{N}^+(i)\}\})) \end{aligned} \quad (9)$$

Similarly for a node with index $i + n \in [n, 2n)$, its neighbors $w = j \in \mathcal{N}_{st}(i)$ in G_{st} map to the inlink-neighbors $j \in \mathcal{N}^-(i - n)$ in G according to Equation 7. The node with index $i + n$ has color label equal to $c_{l,t}^{(t)}$ and the inlink neighbors j , since $j \in [0, n)$ have color labels equal to $c_{l,s}^{(t)}$ (see 8):

$$\begin{aligned} c_l^{(t+1)}(i + n) &= \text{HASH}((c_l^{(t)}(i + 1), \{\{c_l^{(t)}(w) | w \in \mathcal{N}_{st}(i)\}\})) = \\ &= \text{HASH}((c_{l,t}^{(t)}(i), \{\{c_{l,s}^{(t)}(j) | j \in \mathcal{N}^-(i)\}\})) \end{aligned} \quad (10)$$

According to our extension to 1-WL, the refinement we propose reads: $c_{l,s}^{(t+1)}(i) = \text{HASH}((c_{l,s}^{(t)}(i), \{\{c_{l,t}^{(t)}(j) | j \in \mathcal{N}^+(i)\}\}))$ and $c_{l,t}^{(t+1)}(i) = \text{HASH}((c_{l,t}^{(t)}(i), \{\{c_{l,s}^{(t)}(j) | j \in \mathcal{N}^-(i)\}\}))$. By comparing with equations (9) and (10) it follows that $c_{l,s}^{(t+1)} = c_l^{(t+1)}(i)$ and $c_{l,t}^{(t+1)} = c_l^{(t+1)}(i + n)$ which completes the proof. \square

Connecting 1-WL to the encoder layers in DiGAE

We can encode the initial labels $c_i^{(0)}(v)$ of the nodes in our bipartite representation G_{st} by considering two arbitrary, nonequal, vectors \mathbf{s}, \mathbf{t} in $\mathbb{R}^{e \times 1}$ and setting $f^{(0)}(v) = \mathbf{s}^\top$ for nodes $v \in [0, n)$ and $f^{(0)}(v) = \mathbf{t}^\top$ for nodes $v \in [n, 2n)$; e can be as small as 1 (i.e. for one-hot encoding). These encodings are consistent with the initial labels (i.e. they are different for nodes with different initial colors). Given the consistent encodings and our reduction of our color refinement to 1-WL for G_{st} , two results readily apply, from theorems 1 and 2 in Morris et al. (2019). These results readily establish the connection of our 1-WL to 1-GNNs (3).

Alternatively, we can encode the initial labels $c_i^{(0)}(v)$ of the nodes in our bipartite representation G_{st} by vectors $f^{(0)}(v)$ as follows. For nodes $v \in [0, n)$ we assume the encoding $f^{(0)}(v) = [\mathbf{s}^\top, \mathbf{0}]$ and for nodes $v \in [n, 2n)$ we set $f^{(0)}(v) = [\mathbf{0}, \mathbf{t}^\top]$ where $\mathbf{0} \in \mathbb{R}^{1 \times e}$ denotes the zero row vector. Our encodings are in $\mathbb{R}^{1 \times 2e}$ and they are also consistent with our initial labels. In this encoding scheme, the first e elements (last e elements) of the initial feature vector $f^{(0)}(v)$ are non-vanishing for nodes in G_{st} capturing the source (target) role of nodes in G .

We can ensure this property is preserved for feature vectors $f^{(t)}(v), t > 0$ under the iteration in (3) by additionally selecting block-diagonal matrices for $W_1^{(t)}$ and block-antidiagonal matrices for $W_2^{(t)}$:

$$W_1^{(t)} = \begin{pmatrix} W_{1S}^{(t)} & O \\ O & W_{1T}^{(t)} \end{pmatrix}, W_2^{(t)} = \begin{pmatrix} O & W_{2S}^{(t)} \\ W_{2T}^{(t)} & O \end{pmatrix} \quad (11)$$

where $W_{1S}^{(t)}, W_{1T}^{(t)}, W_{2S}^{(t)}, W_{2T}^{(t)} \in \mathbb{R}^{e \times e}$ and $O = O^{e \times e}$ is the zero matrix.

This is straightforward to verify. For a node in $i \in [0, n)$ for which $f^{(t-1)}(i) = [\mathbf{s}_i^{(t-1)}, \mathbf{0}]$ its neighbors $j \in [n, 2n)$ will have encodings of the form $f^{(t-1)}(j) = [\mathbf{0}, \mathbf{t}_j^{(t-1)}]$. Substitution in Equation (3) yields:

$$f^{(t)}(i) = [\sigma(\mathbf{s}_i^{(t-1)\top} \cdot W_{1S}^{(t)} + \sum_{j \in N(i)} \mathbf{t}_j^{(t-1)\top} \cdot W_{2T}^{(t)}), \mathbf{0}^{1 \times e}]$$

so $f^{(t)}(i)$ still has only its *first* e elements non-vanishing, the same as $f^{(t-1)}(i)$. Similarly for $i \in [n, 2n)$ we get: $f^{(t)}(i) = [\sigma(\mathbf{0}^{1 \times e}, \mathbf{t}_i^{(t-1)\top} \cdot W_{1T}^{(t)} + \sum_{j \in N(i)} \mathbf{s}_j^{(t-1)\top} \cdot W_{2S}^{(t)})],$ so $f^{(t)}(i)$ still has only its *last* e elements non-vanishing, the same as $f^{(t-1)}(i)$.

The motivation behind the selection of block-structured parameter matrices $W_1^{(t)}$ and $W_2^{(t)}$, is for allowing the extra flexibility of learning different sets of parameters for nodes with source and target roles (in undirected G_{st}). By removing self-links and setting $W_{1S}^{(t)} = W_{1T}^{(t)} = O^{e \times e}$, these vectors $f^{(t)}(i)$ can be seen to map directly to rows of matrices $\mathbf{S}^{(t)}$ and $\mathbf{T}^{(t)}$ in Equation (6). Alternatively, we can consider general (non-structured) $W_1^{(t)}$ and $W_2^{(t)}$ in our 1-GNN which corresponds to sharing learnt parameters for neural source and target encodings.

Directed Graph AutoEncoder (DiGAE) model

In analogy to the Graph AutoEncoder (GAE) model in Kipf and Welling (2016b), we can define its directed variant (DiGAE) by stacking two directed graph convolutional layers connected with ReLU nonlinearity for its *encoder* and a sigmoid applied to the inner product of the source and target encodings for its *decoder*. In particular, the *encoder* reads

$$\begin{aligned} \mathbf{Z}_S &= \hat{\mathbf{A}} \text{ReLU}(\hat{\mathbf{A}}^\top \mathbf{S}^{(0)} \mathbf{W}_S^{(0)}) \mathbf{W}_T^{(1)} \\ \mathbf{Z}_T &= \hat{\mathbf{A}}^\top \text{ReLU}(\hat{\mathbf{A}} \mathbf{T}^{(0)} \mathbf{W}_T^{(0)}) \mathbf{W}_S^{(1)} \end{aligned} \quad (12)$$

while the decoder for computing the reconstructed adjacency matrix $\bar{\mathbf{A}}$ is

$$\bar{\mathbf{A}} = \sigma(\mathbf{Z}_S \mathbf{Z}_T^\top) \quad (13)$$

In the sequel, we experiment with the single-layer DiGAE model, referred to as *DiGAE-1L*. This autoencoder has the same decoder as DiGAE and its encoder implements the pair of transformations $\mathbf{Z}_S = \mathbf{S}^{(1)} = \hat{\mathbf{A}} \mathbf{T}^{(0)} \mathbf{W}_T^{(0)}$ and $\mathbf{Z}_T = \mathbf{T}^{(1)} = \hat{\mathbf{A}}^\top \mathbf{S}^{(0)} \mathbf{W}_S^{(0)}$.

Related work

Ma et al. (2019) formally extend convolution to directed graphs by defining a normalized, symmetric directed Laplacian and leveraging the Perron vector of the induced transition probability matrix for weighing message passing. In Tong et al. (2020a), Tong et al approximate the digraph Laplacian by means of Personalized PageRank, and this relaxed definition offers performance benefits and the ability to process directed graphs that are not necessarily strongly connected. The authors of Fast Directed GCN in Li et al. (2020) also approximate the digraph Laplacian, by assuming the trivial Perron vector for regular graphs. In Monti et al. (2018), a polynomial of selected motif Laplacians is used to filter node representations. Most notably, all aforementioned spectral-based extensions to convolution in directed graphs, produce single-vector representations, so the dual nature of a node as both a source and target of directed edges is not captured; we do not require the separate computation of the Perron vector and a scheme for weighing messages is automatically learnt. For convolution in directed knowledge graphs, we refer to Kampffmeyer et al. (2019); Schlichtkrull et al. (2018).

In Tong et al. (2020b), first and second order proximity kernels for directed graphs are combined to produce single-vector representations for graph nodes. Second order proximity kernels normalize the products of \mathbf{A} and its transpose, and produce dual-vector intermediate representations, similarly to the work proposed in this paper. However, normalization of the products is graph-agnostic, the intermediate sparse matrix products they employ are computationally costly with potentially dense matrix outputs, the first order proximity kernels is symmetric. High-Order Proximity preserved Embeddings (HOPE) in Ou et al. (2016) rely on matrix factorization (SVD) of a higher order proximity matrix while Asymmetric Proximity Preserving (APP) embeddings in Zhou et al. (2017) rely on random walks with restart. These encoders are not GCN-based which is the focus in our work. Dual-vector representation can be enforced artificially: in Salha et al. (2019), source/target GAE and VGAE models are based on graph auto-encoders for undirected graphs from the seminal work of Kipf and Welling (2016b), where the single-vector representation (of even size) is assumed to be the concatenation of two-identically sized parts. The gravity-inspired directed GCN architecture in Salha et al. (2019) on the other hand produces single vector encodings using fixed normalization for the messages and embeds asymmetry in only one of its entries by fusing the importance of the target node and the distance of the node encodings at the ends of the directed edge.

The directed graph can be of a special kind. Message passing in GCNs for Directed Acyclic Graphs (DAGs) is explored in Thost and Chen (2021). Or the directed edges can carry labels of different types in which case the undirected GCN can be extended to include terms denoting the additional aggregation of edge features Jaume et al. (2019), in close analogy to the extension of WL test to a directed graph with edge labels Orsini et al. (2015); Grohe et al. (2017). In another interesting view, the directed graph can first be converted to an undirected bipartite graph as in Zhou et al. (2005) driven by the source-target node duality.

Experiments

In this section we demonstrate the performance of the proposed approach on the *directed* link prediction task associated with two different datasets: (a) namely CoraML (2,995 nodes, 8,416 edges, 2,879 features), and (b) CiteSeer (3,312 nodes, 4,715 edges, 3,703 features). The CoraML dataset contains machine learning publications grouped into seven classes. The CiteSeer dataset contains scientific papers grouped into six classes. Each paper in CoraML and CiteSeer is represented by a one-hot vector indicating the presence or absence of a word from a dictionary.

We employ grid search for hyperparameter tuning: learning rate $\eta \in \{0.005, 0.01\}$, hidden layer dimension $d \in \{32, 64\}$ with $d/2$ for the latent space dimension, $(\alpha, \beta) \in \{0.0, 0.2, 0.4, 0.6, 0.8\}^2$ for DiGAE models and parameter $\lambda \in \{0.1, 1.0, 10.0\}$ for Gravity GAE. For the final models we select hyperparameter values that maximize mean AUC computed on the validation set. In all cases, models are trained for 200 epochs, using Adam optimizer, without dropout, performing full-batch gradient descent.

We use Python and especially the PyTorch library and PyTorch Geometric Fey and Lenssen (2019), which is a geometric deep learning extension library. We ran experiments for all models (ours and baselines) on a system equipped with an Intel(R) Core(TM) i7-8850H CPU @2.60GHz (6 cores/12 threads) and 32 GB of DDR4 memory @2400 MHz.

We consider the following directed link prediction task adapting the description in Kipf and Welling (2016b) to digraphs.

Task: Directed link prediction We randomly remove 15% of the directed edges from the graph and train models on the remaining edge set. Two thirds of the removed edges (i.e. 10% of all input graph edges) are used as actual edges for testing, one third of them (i.e. 5% of all input graph edges) as actual edges for validation. These test and validation sets also include the same number of fake directed edges (negative samples), as their actual ones: negative samples are

generated by randomly connecting pairs of nodes which are not wired in the input graph. Validation sets are only used for hyperparameter tuning.

Results and Discussion

We compare the performance of our DiGAE models to Standard GAE in Kipf and Welling (2016b), Source/Target GAE and Gravity GAE both in Salha et al. (2019). Similarly to our models, these baselines are GCN-based. We use the TensorFlow implementations of baseline models from the authors of Salha et al. (2019).¹

We run a series of twenty experiments for each graph and selected model combination, and report the mean and standard deviation of the AUC and AP metrics, as well as their respective timings. Random train and test graph dataset splits are used for each such experiment and metrics are averaged over the set, to account for their sensitivity to the choice of the split, as empirically observed in Shchur et al. (2018).

Results with node features supplied in all cases (feature-based configurations), are summarized in Table 1. We mark in bold the largest entry (or largest entries in the case of their overlapping intervals).

Mean AUC values for DiGAE-1L in particular consistently outperform other baselines for the citation graphs and the margin can be significant: in CiteSeer this is of the order of 6% for Gravity GAE and up to 18% compared to Standard GAE. For mean AP, margins are similarly in the 4% to 19% range, or up to 3% for CoraML. Varying (α, β) pair values has significant impact on the reconstruction metrics. As an example, the mean AUC can be as low as 73.73% and 86.10% for DiGAE-1L respectively for CoraML and CiteSeer for the selected η and d but for suboptimal (α, β) within the search grid. In the Appendix we include metrics tables for the full (α, β) grid collected during hyperparameter tuning. In experiments with citation graphs, DiGAE-1L is markedly faster by factors in the range $\times 5$ to $\times 15$. This is partly due to the different implementations, the fact that this is a single-layer only and for CiteSeer in particular to the smaller size for the output vector from hyperparameter tuning (16 vs 32 for a hidden encoding of 64 entries for baselines). Gravity GAE is the slowest, mainly due to the complexity of its decoder (pairwise distance computation).

The authors in Salha et al. (2019) originally used the baselines with one-hot encoding of the nodes (feature-less configurations). For citation networks, node features capture similarity which is symmetric and this could conceptually hinder the identification of directionality in predicted links as in our task, which is an inherently asymmetric relation. For this reason, we also tested feature-less configurations for the baselines and interestingly got comparable results to the feature-based case (Table 2): our DiGAE-1L models from (Table 1) are top performers for both CoraML and CiteSeer datasets. Experiments with datasets from the WebKB collection and Pubmed are included in the Appendix.

Table 1: General directed link prediction for the *citation* graphs (feature-based configurations).

Dataset	Model	AUC	AP	Time (secs)
CoraML	DiGAE (ours)	88.10 +/- 1.70	89.83 +/- 1.39	9.56 +/- 0.48
CoraML	DiGAE 1-Layer (ours)	94.09 +/- 0.66	94.10 +/- 0.77	7.64 +/- 0.21
CoraML	Gravity GAE	92.35 +/- 0.57	94.17 +/- 0.53	51.56 +/- 0.13
CoraML	Source/Target GAE	91.66 +/- 0.52	92.60 +/- 0.47	36.88 +/- 0.20
CoraML	Standard GAE	89.54 +/- 1.14	91.40 +/- 1.11	36.55 +/- 0.21
CiteSeer	DiGAE (ours)	92.05 +/- 1.06	92.29 +/- 0.97	11.10 +/- 0.22
CiteSeer	DiGAE 1-Layer (ours)	92.76 +/- 0.87	92.57 +/- 1.08	4.12 +/- 0.11
CiteSeer	Gravity GAE	86.79 +/- 0.98	88.60 +/- 1.05	106.44 +/- 0.16
CiteSeer	Source/Target GAE	82.90 +/- 1.79	84.70 +/- 1.47	73.46 +/- 0.21
CiteSeer	Standard GAE	74.35 +/- 1.77	80.96 +/- 1.26	73.84 +/- 0.48

Truncated SVD baseline We also explore the performance of an approach based on truncated SVD for our directed link prediction task. For a given train/validation/test split, we use the directed edges that are available to use for training for building a *partial* adjacency matrix A_p of the underlying directed graph $G(V, E)$ and compute its truncated SVD, retaining the singular triplets corresponding to its largest k singular values, $A_p \approx U_k \Sigma_k V_k^T$. Then we consider the matrices for the source and target encodings of nodes $Z_S = U_k \Sigma_k^{1/2}$ and $Z_T = V_k \Sigma_k^{1/2}$ and use the asymmetric decoder from Equation (13) for predicting directed links. We use the same evaluation pipeline as in our GNN experiments and compute respective AUC and AP performance metrics for the graph reconstruction. For truncated SVD we

¹https://github.com/deezer/gravity_graph_autoencoders

Table 2: General directed link prediction for the *citation* graphs (feature-less configurations).

Dataset	Model	AUC	AP
CoraML	Gravity GAE	91.56 +/- 0.71	93.62 +/- 0.59
CoraML	Source/Target GAE	91.85 +/- 0.58	92.91 +/- 0.64
CoraML	Standard GAE	89.42 +/- 0.84	92.09 +/- 0.64
CiteSeer	Gravity GAE	87.05 +/- 0.99	88.88 +/- 0.96
CiteSeer	Source/Target GAE	82.39 +/- 1.56	84.38 +/- 1.57
CiteSeer	Standard GAE	73.81 +/- 1.37	80.52 +/- 1.13

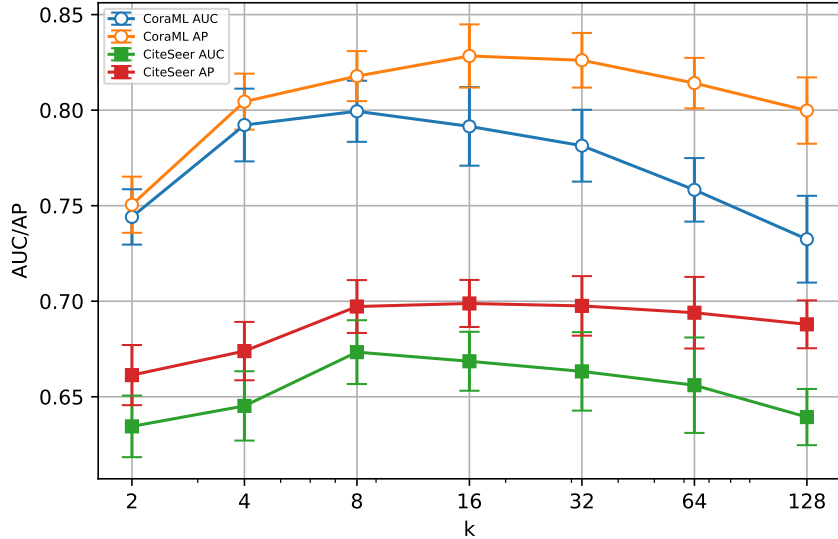


Figure 2: Truncated SVD based directed link prediction: AUC and AP metrics for CoraML and CiteSeer.

experimented with implementations based on ARPACK Lehoucq et al. (1998) and randomized SVD Halko et al. (2011) for $k \in \{2^i | i = 1, 2, \dots, 7\}$ and we got very similar metrics for our input graphs (please refer to the Appendix for metrics tables). We repeated for 20 random graph splits for each graph, k and implementation combination. Figure 2 summarizes the results for the *largest* mean AUC and AP value for each graph, k combination. We observe that for 16-dimensional encoding vectors we get best results in reconstruction in terms of mean AP: 82.83% for CoraML and 69.88% for CiteSeer. These are significantly lower than 94.10% for CoraML and 92.57% for CiteSeer that the “neural” source and target encodings our DiGAE-1L produces. SVD encodes only connectivity while DiGAE models, being GNNs, leverage both connectivity *and* node features. The truncated SVD baseline is essentially the HOPE idea Ou et al. (2016) with the proximity matrix being the adjacency matrix \mathbf{A} . For comparison and for the standard Katz proximity in HOPE, $(\mathbf{I} - \beta\mathbf{A})^{-1}\beta\mathbf{A}$, we computed *largest* mean AP values in reconstruction over $k \in \{2^i | i = 1, 2, \dots, 7\}$, $\beta = 0.02$, applying 20 random graph splits for each k . We get 83.87% for CoraML and 67.29% for CiteSeer: comparable to truncated SVD baseline results and significantly lower than the respective DiGAE-1L metrics. We include tables with detailed results in the Appendix.

Clustering source and target encodings We used t-Distributed Stochastic Neighbor Embedding (t-SNE) Van der Maaten and Hinton (2008) for reducing the dimension of source and target representations of nodes produced by DiGAE in order to visualize them. Figure 3 illustrates a crisp separation of points with different class labels and this is true for both source and target vectors. This separation is not present in their feature space. This implies that DiGAE embeddings are promising inputs for clustering purposes. The fact that the clusters can be independently identified in both the source and target space opens up the possibility for exploring sets of points that share cluster identity in both spaces, as the core ones for a label.

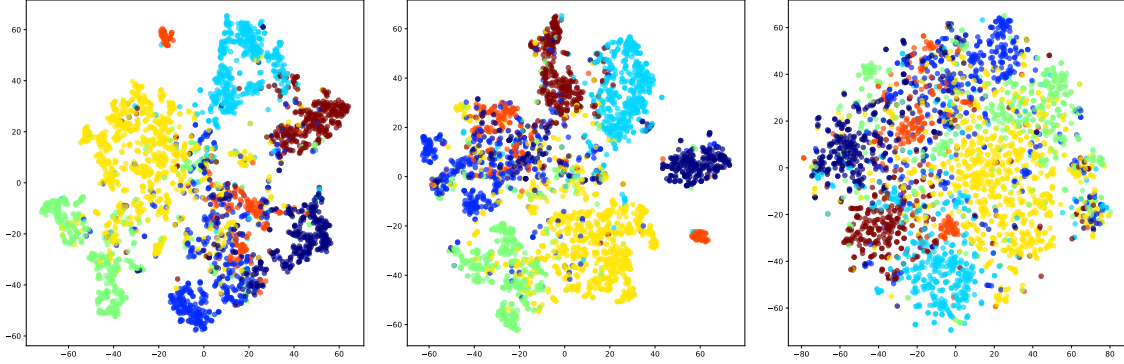


Figure 3: Left and center: t-SNE embeddings on source and target representations computed with our DiGAE-1L for CoraML. Right: embeddings of original feature vectors (colors indicate classes).

Vector hub and authority scores Source and target representations are expected to be the (vector) surrogates respectively of (scalar) hub and authority scores. Table 3 confirms this intuition. A source vector of particularly large magnitude for a node a will be more probable to yield large inner products with target vectors of other nodes b in the decoder. This means that a directed edge $a \mapsto b$ will be likely to appear, which will increase a 's outdegree. Similarly, a large magnitude for a node's target vector encourages other nodes to connect to it and increase its indegree. In turn, outdegrees are known to correlate to hub scores and indegrees to authority and PageRank scores.

Table 3: Pearson correlation coefficients between the magnitudes of source and target vector encodings, and a collection of centrality scores (Hub/Authority and PageRank) and degrees (in/out), for all nodes in CoraML. Encodings were computed with DiGAE-1L.

	source magnitude	target magnitude
hub	0.37	0.06
outdegree	0.82	0.12
authority	0.05	0.41
pagerank	-0.01	0.48
indegree	0.08	0.77

Conclusions and future work

In this paper we present DiGAE, a new class of directed graph autoencoders that computes a pair of vector representations for each node. It exploits the asymmetry in input and output node degrees and further skews this by allowing exponents in scaling the features to enter as parameters. DiGAE outperforms state-of-the art GCN-based graph autoencoders on the directed link prediction task and can be an order of magnitude times faster in learning representations for CoraML and CiteSeer datasets. In future work, we plan to explore encoders that integrate scaling decisions that are *local* to each node.

Appendix

We include the detailed algorithm for WL and the message passing view of a simplified GCN layer. We then describe our coloring of pairs of node labels in directed graphs and its associated message passing scheme.

In order to emphasize the impact of α and β hyperparameters on performance metrics for CoarML and CiteSeer datasets, we visualize AUC mean values, collected during hyperparameter tuning, for the *selected* model’s η and d values. We also provide the detailed performance metrics table for the truncated SVD baseline for both standard and randomized SVD implementations on which Figure 2 in the main text is based and the standard Katz proximity in HOPE is similarly explored next. An application of all models on small Web graphs from the WebKB collection follows. We conclude with experiments over a larger dataset, Pubmed, in which we confirm the performance benefits of our DiGAE models and the optimization opportunities that parameters α , β offer, followed by a short note connecting them to the spectral modifications they effect.

Weisfeiler-Leman (WL) algorithm

Algorithm 1 provides a summary of the Weisfeiler-Leman (WL) algorithm.

Algorithm 1 Weisfeiler-Leman (WL) algorithm

Input: Neighbor lists $\mathcal{N}(i)$, for all nodes $i \in [0, n)$
 Ensure neighbor lists are lexicographically sorted: $\mathcal{N}(i) \leftarrow \text{sort}(\mathcal{N}(i)), \forall i \in [0, n)$
 Initialize: $k \leftarrow 0$; $l_i^{(k)} := c$ (same label), $h_i^{(k)} := \text{hash}(i), \forall i \in [0, n)$; $L^{(0)} := \{l_i^{(0)} : i \in [0, n)\}$
while True **do**
 Hash the tuple of (sorted) neighbors’ labels: $h_i^{(k+1)} := \text{hash}(\langle l_j^{(k)} : j \in \mathcal{N}(i) \rangle)$
 List of unique hashes \mathcal{H} : $\mathcal{H} \leftarrow \text{sort}(\{\{h_i^{(k+1)} : i \in [0, n)\}\})$
 Function f maps items in \mathcal{H} to labels: $f(\mathcal{H}_j) := j, \forall j \in [0, \text{size}(\mathcal{H}))$
 Update labels: $l_i^{(k+1)} := f(h_i^{(k+1)}), \forall i \in [0, n)$
 Update set of labels: $L^{(k+1)} := \{l_i^{(k+1)} : i \in [0, n)\}$
 if $L^{(k+1)} = L^{(k)}$ **then**
 break
 else
 $k \leftarrow k + 1$
 end if
end while
Output: $L^{(k)}$

GCNs as message passing systems

Algorithm 2 describes the steps each node i performs to update its current encoding \mathbf{x}_i given the set of its neighbors $\mathcal{N}(i)$ and a transformation matrix \mathbf{W} (which is identical for all nodes).

Coloring of pairs of node labels in directed graphs

Algorithm 3 provides a summary of our extension of 1-WL for directed graphs.

DiGAE encoder layer as a message passing system

We can express our DiGAE encoder layer in a message-passing fashion; Algorithm 4 details the operations performed at each node i .

Algorithm 2 Updating the encoding of node i in a GCN layer

Input: $\mathbf{x}_i, \mathcal{N}(i), \mathbf{W}$
 Set: $\tilde{\mathcal{N}}(i) := \mathcal{N}(i) \cup \{i\}$ and $\text{deg}(i) := |\tilde{\mathcal{N}}(i)|$
 Transform: $\mathbf{x}_i \leftarrow \mathbf{W}^\top \mathbf{x}_i$
 Scale: $\mathbf{x}_i \leftarrow \frac{1}{\sqrt{\text{deg}(i)}} \mathbf{x}_i$
 Send: $\text{send}(\mathbf{x}_i, j)$ to all nodes $j \in \tilde{\mathcal{N}}(i)$
 Receive: $\mathbf{x}_j \leftarrow \text{receive}(j)$ from all nodes $j \in \tilde{\mathcal{N}}(i)$
 Sum: $\mathbf{x}_i \leftarrow \sum_{j \in \tilde{\mathcal{N}}(i)} \mathbf{x}_j$
 Scale: $\mathbf{x}_i \leftarrow \frac{1}{\sqrt{\text{deg}(i)}} \mathbf{x}_i$
Output: \mathbf{x}_i

Algorithm 3 Coloring of pairs of node labels in directed graphs

Input: Neighbor lists for outgoing and incoming edges, $\mathcal{N}^+(i)$ and $\mathcal{N}^-(i)$ respectively, for all nodes $i \in [0, n)$
 Ensure neighbor lists are lexicographically sorted: $\mathcal{N}^+(i) \leftarrow \text{sort}(\mathcal{N}^+(i)), \mathcal{N}^-(i) \leftarrow \text{sort}(\mathcal{N}^-(i)), \forall i \in [0, n)$
 Initialize: $t \leftarrow 0; c_{i,s}^{(t)} := \mathbf{s}, c_{i,t}^{(t)} := \mathbf{t}; h_s^{(t)}(i) = \text{HASH}(\mathbf{s}), h_t^{(t)}(i) := \text{HASH}(\mathbf{t}), \forall i \in [0, n); L_s^{(0)} = L_t^{(0)} := \{\mathbf{s}, \mathbf{t}\}$
while True **do**
 Hash *source* label, *target* labels of pointed nodes: $h_s^{(t+1)}(i) := \text{HASH}(c_{i,s}^{(t)}(i), \langle c_{i,t}^{(t)}(j) : j \in \mathcal{N}^+(i) \rangle)$
 Hash node *target* label, *source* labels of pointing nodes: $h_t^{(t+1)}(i) := \text{HASH}(c_{i,t}^{(t)}(i), \langle c_{i,s}^{(t)}(j) : j \in \mathcal{N}^-(i) \rangle)$
 List of unique hashes for nodes with *source* role: $\mathcal{H}_s: \mathcal{H}_s \leftarrow \text{sort}(\{h_s^{(t+1)}(i) : i \in [0, n)\})$
 List of unique hashes for nodes with *target* role: $\mathcal{H}_t: \mathcal{H}_t \leftarrow \text{sort}(\{h_t^{(t+1)}(i) : i \in [0, n)\})$
 Function f_s maps items in \mathcal{H}_s to labels: $f_s(\mathcal{H}_s(j)) := j, \forall j \in [0, \text{size}(\mathcal{H}_s))$
 Function f_t maps items in \mathcal{H}_t to labels: $f_t(\mathcal{H}_t(j)) := j, \forall j \in [0, \text{size}(\mathcal{H}_t))$
 Update *source* labels: $c_{i,s}^{(t+1)}(i) := f_s(h_s^{(t+1)}(i)), \forall i \in [0, n)$
 Update *target* labels: $c_{i,t}^{(t+1)}(i) := f_t(h_t^{(t+1)}(i)), \forall i \in [0, n)$
 Update sets of labels: $L_s^{(t+1)} := \{c_{i,s}^{(t+1)}(i) : i \in [0, n)\}; L_t^{(t+1)} := \{c_{i,t}^{(t+1)}(i) : i \in [0, n)\}$
 if $L_s^{(t+1)} = L_s^{(t)}$ and $L_t^{(t+1)} = L_t^{(t)}$ **then**
 break
 else
 $t \leftarrow t + 1$
 end if
end while
Output: $L_s^{(t)}, L_t^{(t)}$

Algorithm 4

Input: $\mathbf{s}_i, \mathbf{t}_i; \mathcal{N}^+(i), \mathcal{N}^-(i); \mathbf{W}_S, \mathbf{W}_T; \alpha, \beta$
 Set: $\tilde{\mathcal{N}}^+(i) := \mathcal{N}^+(i) \cup \{i\}$ and $\text{deg}^+(i) := |\tilde{\mathcal{N}}^+(i)|; \tilde{\mathcal{N}}^-(i) := \mathcal{N}^-(i) \cup \{i\}$ and $\text{deg}^-(i) := |\tilde{\mathcal{N}}^-(i)|$
 Transform: $\mathbf{s}_i \leftarrow \mathbf{W}_S^\top \mathbf{s}_i; \mathbf{t}_i \leftarrow \mathbf{W}_T^\top \mathbf{t}_i;$
 Scale: $\mathbf{s}_i \leftarrow \frac{1}{(\text{deg}^+(i))^\beta} \mathbf{s}_i; \mathbf{t}_i \leftarrow \frac{1}{(\text{deg}^-(i))^\alpha} \mathbf{t}_i$
 Send: $\text{send}(\mathbf{s}_i, j)$ to all nodes $j \in \tilde{\mathcal{N}}^+(i); \text{send}(\mathbf{t}_i, j)$ to all nodes $j \in \tilde{\mathcal{N}}^-(i)$
 Receive: $\mathbf{s}_j \leftarrow \text{receive}(j)$ from all nodes $j \in \tilde{\mathcal{N}}^+(i); \mathbf{t}_j \leftarrow \text{receive}(j)$ from all nodes $j \in \tilde{\mathcal{N}}^-(i)$
 Sum: $\mathbf{s}_i \leftarrow \sum_{j \in \tilde{\mathcal{N}}^+(i)} \mathbf{s}_j; \mathbf{t}_i \leftarrow \sum_{j \in \tilde{\mathcal{N}}^-(i)} \mathbf{t}_j$
 Scale: $\mathbf{s}_i \leftarrow \frac{1}{(\text{deg}^+(i))^\beta} \mathbf{s}_i; \mathbf{t}_i \leftarrow \frac{1}{(\text{deg}^-(i))^\alpha} \mathbf{t}_i$
Output: $\mathbf{s}_i, \mathbf{t}_i$

CoraML and CiteSeer datasets

Impact of α and β on the performance for DiGAE models

Figure 4 lists the mean AUC scores of the *DiGAE* model for various combinations of the hyperparameters (α, β) . Numbers inside the boxes are mean AUC values collected during hyperparameter tuning, for the η and d values of the *selected* model.

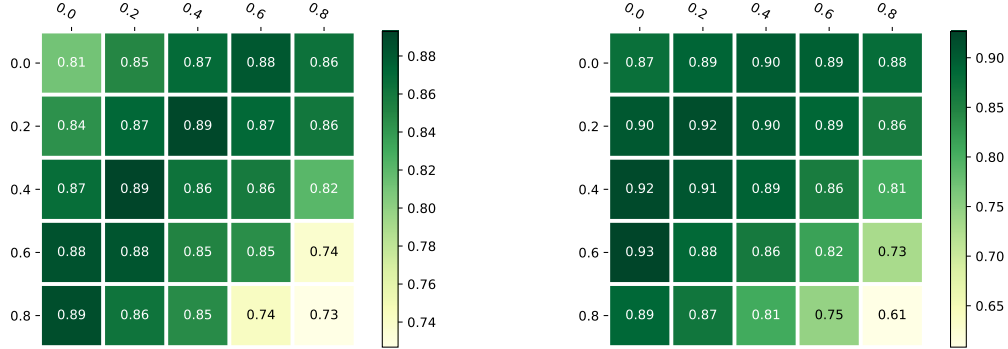


Figure 4: Grid search for CoraML (left) and CiteSeer (right) datasets to identify optimal α (vertical) and β (horizontal) for DiGAE model. Numbers inside the boxes indicate respective AUC scores.

Figure 5 is the analogous for Figure 4, but for the *DiGAE-IL* model.

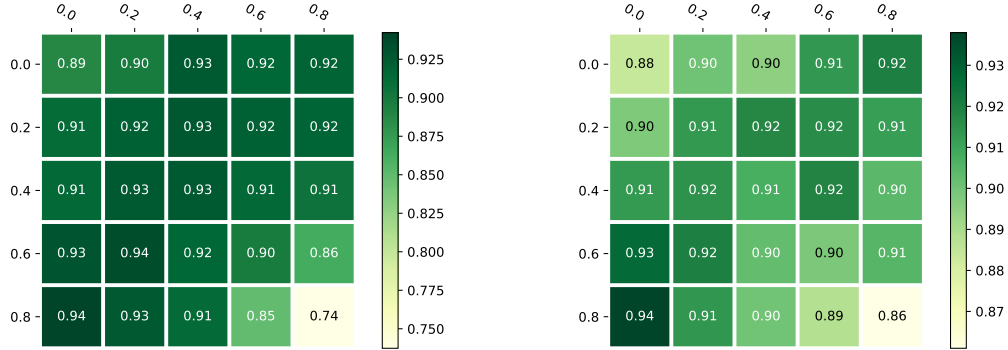


Figure 5: Grid search for CoraML (left) and CiteSeer (right) datasets to identify optimal α (vertical) and β (horizontal) for DiGAE-IL model. Numbers inside the boxes indicate respective AUC scores.

Truncated SVD baseline metrics

Table 4 details the metrics obtained in the truncated SVD baseline experiments.

HOPE baselines

For comparison and for the standard Katz proximity $(\mathbf{I} - \beta\mathbf{A})^{-1}\beta\mathbf{A}$ in HOPE Ou et al. (2016), we computed AUC and AP metrics for $k \in \{2^i | i = 1, 2, \dots, 7\}$, $\beta = 0.02$, 20 random splits, for CoraML and CiteSeer datasets. Table 5 details the metrics obtained in the experiments.

Results on WebKB collection datasets

We experiment with the following datasets from the WebKB collection²: “Wisconsin”, “Texas” and “Cornell”; their properties are in Table 6. In WebKB datasets, nodes represent Web pages and are manually classified into the five

²<http://www.cs.cmu.edu/afs/cs.cmu.edu/project/theo-11/www/wwkb/>

Table 4: Truncated SVD baseline metrics (AUC and AP) for CoraML and CiteSeer datasets: two SVD implementations (standard and randomized) and different encoding vector sizes: $k = 2, 4, 8, 16, 32, 64, 128$.

Dataset	Model	k	AUC	AP
CoraML	SVD	2	74.41 +/- 1.45	75.05 +/- 1.47
CoraML	SVD	4	79.22 +/- 1.90	80.45 +/- 1.47
CoraML	SVD	8	79.94 +/- 1.60	81.78 +/- 1.31
CoraML	SVD	16	78.79 +/- 1.35	81.61 +/- 1.35
CoraML	SVD	32	77.91 +/- 1.71	81.84 +/- 1.47
CoraML	SVD	64	75.23 +/- 1.33	80.76 +/- 1.09
CoraML	SVD	128	70.79 +/- 1.70	78.03 +/- 1.12
CoraML	RandSVD	2	72.62 +/- 2.64	76.11 +/- 2.02
CoraML	RandSVD	4	75.85 +/- 1.75	78.91 +/- 1.35
CoraML	RandSVD	8	78.09 +/- 1.08	81.36 +/- 1.15
CoraML	RandSVD	16	79.15 +/- 2.06	82.83 +/- 1.65
CoraML	RandSVD	32	78.14 +/- 1.88	82.61 +/- 1.43
CoraML	RandSVD	64	75.83 +/- 1.66	81.41 +/- 1.32
CoraML	RandSVD	128	73.25 +/- 2.27	79.98 +/- 1.74
CiteSeer	SVD	2	61.62 +/- 1.26	61.84 +/- 1.17
CiteSeer	SVD	4	62.23 +/- 1.31	62.62 +/- 1.34
CiteSeer	SVD	8	63.76 +/- 1.41	64.36 +/- 1.25
CiteSeer	SVD	16	62.84 +/- 1.59	63.88 +/- 1.42
CiteSeer	SVD	32	63.11 +/- 1.44	64.42 +/- 1.44
CiteSeer	SVD	64	62.51 +/- 1.60	64.31 +/- 1.39
CiteSeer	SVD	128	63.51 +/- 1.93	65.81 +/- 1.64
CiteSeer	RandSVD	2	63.45 +/- 1.61	66.13 +/- 1.57
CiteSeer	RandSVD	4	64.52 +/- 1.81	67.39 +/- 1.53
CiteSeer	RandSVD	8	67.34 +/- 1.67	69.72 +/- 1.38
CiteSeer	RandSVD	16	66.86 +/- 1.54	69.88 +/- 1.23
CiteSeer	RandSVD	32	66.33 +/- 2.05	69.76 +/- 1.56
CiteSeer	RandSVD	64	65.61 +/- 2.50	69.40 +/- 1.87
CiteSeer	RandSVD	128	63.94 +/- 1.47	68.79 +/- 1.25

categories: student, project, course, staff, and faculty; edges are hyperlinks between them. Node features are the bag-of-words representation of the Web pages. We apply the same pipeline as for CoraML and CiteSeer citation datasets. In Table 7 we report the performance metrics for the case the node features are input in model training. For the feature-less configurations, performance of baselines is reported in Table 8.

Likewise for citation datasets, both DiGAE models perform better in mean AUC and AP for all WebKB networks. Note however that performance metrics for any model over different splits for these small graphs have large standard deviations, which does not provide a clean performance ranking of the models.

Results on Pubmed dataset

We experiment with the Pubmed dataset (19,717 nodes, 44,338 edges, 500 features) which is a citation network pertaining to diabetes classified into one of three classes (“Diabetes Mellitus, Experimental”, “Diabetes Mellitus Type 1”, “Diabetes Mellitus Type 2”)³.

We employ the same grid search strategy for hyperparameter tuning and training setup as for other citation datasets. We report on the mean AUC and AP metrics and their respective timings over a series of ten experiments for each selected model, with one hot-encoding of the nodes (feature-less configurations), in Table 9. DiGAE models consistently and significantly outperform other baselines by margins which are in the 7% to 13% range for mean AUC and in the 4% to 8% range for mean AP; they are also considerably faster. DiGAE-1L in particular is the fastest overall by a factor close or exceeding $\times 10$ and performs best overall in the mean AUC and AP metrics.

³<https://lincs.soe.ucsc.edu/data>

Table 5: HOPE baseline metrics (AUC and AP) for CoraML and CiteSeer datasets and for different encoding vector sizes: $k = 2, 4, 8, 16, 32, 64, 128$. Katz Index proximity has its β parameter set to 0.02.

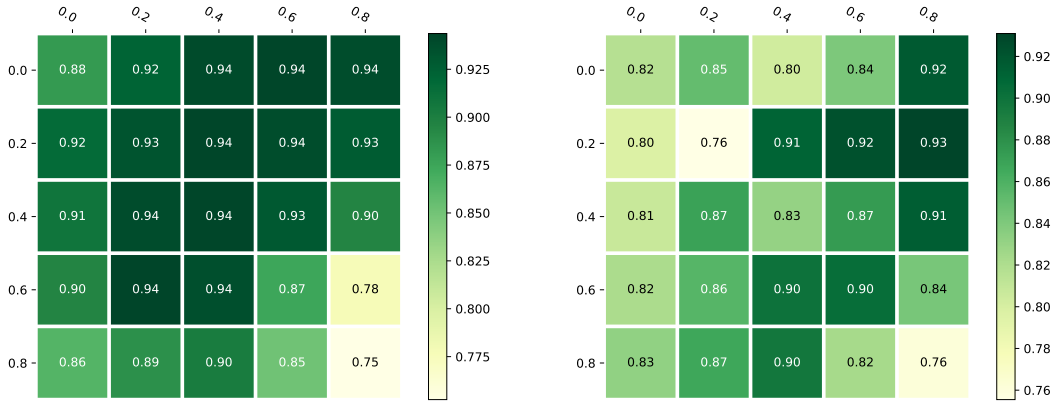
Dataset	Model	k	AUC	AP
CoraML	HOPE/Katz	2	71.24 +/- 1.09	72.08 +/- 1.23
CoraML	HOPE/Katz	4	79.27 +/- 1.53	80.18 +/- 1.35
CoraML	HOPE/Katz	8	81.38 +/- 1.50	82.49 +/- 1.47
CoraML	HOPE/Katz	16	79.47 +/- 1.40	82.05 +/- 1.18
CoraML	HOPE/Katz	32	80.77 +/- 1.50	83.87 +/- 1.23
CoraML	HOPE/Katz	64	78.08 +/- 1.41	82.45 +/- 1.16
CoraML	HOPE/Katz	128	75.00 +/- 1.95	80.91 +/- 1.38
CiteSeer	HOPE/Katz	2	60.64 +/- 1.27	60.75 +/- 1.25
CiteSeer	HOPE/Katz	4	62.14 +/- 1.66	62.56 +/- 1.58
CiteSeer	HOPE/Katz	8	63.66 +/- 1.49	64.06 +/- 1.46
CiteSeer	HOPE/Katz	16	64.17 +/- 1.69	65.05 +/- 1.62
CiteSeer	HOPE/Katz	32	63.72 +/- 1.47	65.10 +/- 1.44
CiteSeer	HOPE/Katz	64	64.33 +/- 2.24	66.03 +/- 1.89
CiteSeer	HOPE/Katz	128	65.07 +/- 1.36	67.29 +/- 1.27

Table 6: WebKB datasets.

Dataset	Number of nodes	Number of edges	Number of features
Texas	183	325	1703
Cornell	183	298	1703
Wisconsin	251	515	1703

Impact of α and β on the performance for DiGAE models

In Figure 6 we list the mean AUC scores of the *DiGAE* models for various combinations of hyperparameters (α, β) for the Pubmed dataset. Numbers inside the boxes are mean AUC values collected during hyperparameter tuning, for the η and d values of the *selected* model. We confirm the flexibility to further optimize performance metrics by suitably tuning node degrees' exponentiation parameters α and β .

Figure 6: Grid search for Pubmed dataset to identify optimal α (vertical) and β (horizontal) for DiGAE-1L (left pane) and DiGAE (right pane) models. Numbers inside the boxes indicate respective AUC scores.

A note on the role of parameters α and β .

By varying exponent parameters α and β we modify the spectrum (singular values) of our multiplication matrices $\hat{\mathbf{A}}, \hat{\mathbf{A}}^\top$ (please see Equations (6) in the text). In particular for smaller parameter values, the scaling role of the node degrees d is suppressed (and in the limit of 0 it vanishes: $1/d^0 = 1$) and the spectrum max shifts to larger values while

Table 7: General directed link prediction for the *WebKB* graphs (feature-based configurations).

Dataset	Model	AUC	AP	Time (secs)
Wisconsin	DiGAE (ours)	73.95 +/- 7.55	79.64 +/- 6.31	1.12 +/- 0.04
Wisconsin	DiGAE 1-Layer (ours)	81.14 +/- 7.36	85.60 +/- 5.03	0.82 +/- 0.03
Wisconsin	Gravity GAE	73.37 +/- 4.19	76.73 +/- 3.97	0.70 +/- 0.10
Wisconsin	Source/Target GAE	72.73 +/- 5.31	78.40 +/- 4.17	0.56 +/- 0.04
Wisconsin	Standard GAE	67.84 +/- 5.02	75.34 +/- 4.28	0.51 +/- 0.10
Texas	DiGAE (ours)	64.79 +/- 17.24	74.38 +/- 12.99	0.93 +/- 0.03
Texas	DiGAE 1-Layer (ours)	70.58 +/- 8.16	76.97 +/- 7.82	0.69 +/- 0.03
Texas	Gravity GAE	64.14 +/- 7.98	71.38 +/- 7.41	0.56 +/- 0.08
Texas	Source/Target GAE	63.50 +/- 7.41	68.42 +/- 6.72	0.47 +/- 0.05
Texas	Standard GAE	50.80 +/- 7.93	62.28 +/- 5.60	0.46 +/- 0.05
Cornell	DiGAE (ours)	69.69 +/- 12.07	77.14 +/- 9.77	0.90 +/- 0.03
Cornell	DiGAE 1-Layer (ours)	61.96 +/- 10.27	70.69 +/- 10.26	0.65 +/- 0.02
Cornell	Gravity GAE	66.24 +/- 4.84	69.10 +/- 5.01	0.59 +/- 0.09
Cornell	Source/Target GAE	62.82 +/- 5.75	69.42 +/- 5.25	0.47 +/- 0.05
Cornell	Standard GAE	57.49 +/- 7.78	68.72 +/- 6.54	0.47 +/- 0.05

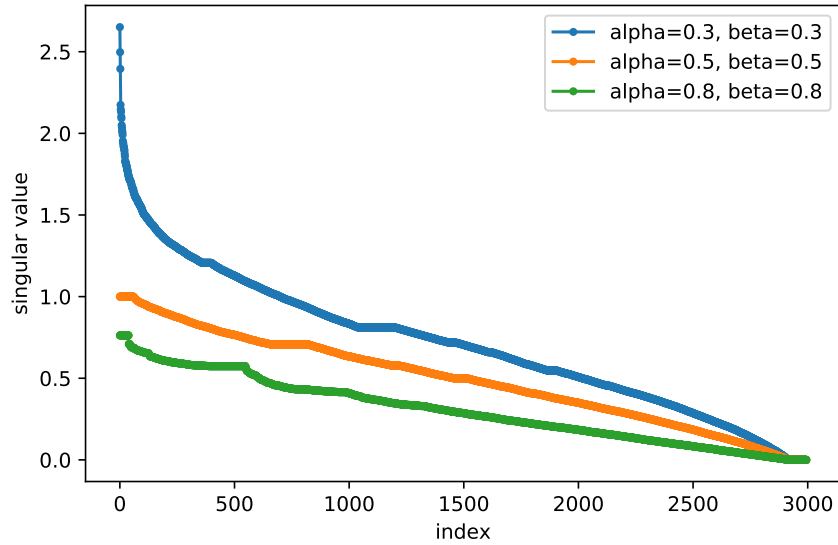
Table 8: General directed link prediction for the *WebKB* graphs (feature-less configurations).

Dataset	Model	AUC	AP
Wisconsin	Gravity GAE	67.04 +/- 5.35	74.41 +/- 4.42
Wisconsin	Source/Target GAE	72.46 +/- 5.89	77.05 +/- 5.68
Wisconsin	Standard GAE	65.89 +/- 5.28	74.00 +/- 4.13
Texas	Gravity GAE	65.53 +/- 7.30	70.77 +/- 6.47
Texas	Source/Target GAE	62.37 +/- 5.24	67.58 +/- 4.13
Texas	Standard GAE	53.81 +/- 6.61	64.24 +/- 5.27
Cornell	Gravity GAE	69.58 +/- 5.26	73.41 +/- 5.07
Cornell	Source/Target GAE	65.14 +/- 5.71	69.90 +/- 5.18
Cornell	Standard GAE	60.26 +/- 7.96	69.21 +/- 6.91

for larger parameters the spectrum range shrinks. Spectrum shrinking will typically lead to smaller magnitudes for source and target encodings from Equations (6) (and their respective inner products) and so the sigmoid function in the decoder can fail to predict links: this is consistent with the particularly low performance metrics when both α and β are large. Please see the spectrum for CoraML’s $\hat{\mathbf{A}}$ for $\alpha, \beta \in \{0.3, 0.5, 0.8\}, \alpha = \beta$ in Figure 7. From the local smoothing perspective around a node i , smaller α ’s reinforce the role of "authority" nodes j pointed to by i (i.e. nodes with large indegree $\text{deg}^-(j)$) in updating source encoding \mathbf{s}_i from \mathbf{t}_j ’s (contributing terms analogous to $\frac{1}{\text{deg}^-(j)^\alpha} \mathbf{t}_j$). Similarly, smaller β ’s reinforce the role of "hub" nodes j pointing to i (i.e. nodes with large outdegree $\text{deg}^+(j)$) in updating target encoding \mathbf{t}_i from \mathbf{s}_j ’s (contributing terms analogous to $\frac{1}{\text{deg}^+(j)^\beta} \mathbf{s}_j$). For a deeper theoretical analysis of the impact of the parameters on the spectrum, the simplified linear case (as in "Simplifying Graph Convolutional Networks", Wu et al (2019), there for the impact of self-links) could be a starting point and this is deferred for future research.

Table 9: General directed link prediction for *Pubmed* dataset (feature-less configurations).

Dataset	Model	AUC	AP	Time (secs)
Pubmed	DiGAE (ours)	92.09 +/- 1.92	91.08 +/- 1.22	98.62 +/- 2.75
Pubmed	DiGAE 1-Layer (ours)	94.35 +/- 0.37	93.16 +/- 0.48	45.49 +/- 0.48
Pubmed	Gravity GAE	84.28 +/- 0.59	86.60 +/- 0.58	560.09 +/- 9.94
Pubmed	Source/Target GAE	85.01 +/- 1.36	87.28 +/- 0.60	418.40 +/- 2.13
Pubmed	Standard GAE	81.43 +/- 0.32	85.88 +/- 0.31	421.56 +/- 5.95

Figure 7: Spectrum for CoraML's $\hat{\mathbf{A}}$ for $\alpha, \beta \in \{0.3, 0.5, 0.8\}, \alpha = \beta$.

References

- Justin Gilmer, Samuel S Schoenholz, Patrick F Riley, Oriol Vinyals, and George E Dahl. Neural message passing for quantum chemistry. In *International Conference on Machine Learning*, pages 1263–1272. PMLR, 2017.
- Alessio Micheli. Neural network for graphs: A contextual constructive approach. *IEEE Transactions on Neural Networks*, 20(3):498–511, 2009.
- Mathias Niepert, Mohamed Ahmed, and Konstantin Kutzkov. Learning convolutional neural networks for graphs. In *International conference on machine learning*, pages 2014–2023. PMLR, 2016.
- Petar Veličković, Guillem Cucurull, Arantxa Casanova, Adriana Romero, Pietro Liò, and Yoshua Bengio. Graph attention networks. *6th International Conference on Learning Representations*, 2017.
- Joan Bruna, Wojciech Zaremba, Arthur Szlam, and Yann LeCun. Spectral networks and deep locally connected networks on graphs. In *2nd International Conference on Learning Representations, ICLR 2014*, 2014.
- Michaël Defferrard, Xavier Bresson, and Pierre Vandergheynst. Convolutional neural networks on graphs with fast localized spectral filtering. In *Proceedings of the 30th International Conference on Neural Information Processing Systems*, pages 3844–3852, 2016.
- Thomas N Kipf and Max Welling. Semi-supervised classification with graph convolutional networks. *arXiv preprint arXiv:1609.02907*, 2016a.
- Mingdong Ou, Peng Cui, Jian Pei, Ziwei Zhang, and Wenwu Zhu. Asymmetric transitivity preserving graph embedding. In *Proceedings of the 22nd ACM SIGKDD international conference on Knowledge discovery and data mining*, pages 1105–1114, 2016.
- Boris Weisfeiler and Andrei Leman. The reduction of a graph to canonical form and the algebra which appears therein. *NTI, Series*, 2(9):12–16, 1968.
- David K Hammond, Pierre Vandergheynst, and Rémi Gribonval. Wavelets on graphs via spectral graph theory. *Applied and Computational Harmonic Analysis*, 30(2):129–150, 2011.
- Christopher Morris, Martin Ritzert, Matthias Fey, William L Hamilton, Jan Eric Lenssen, Gaurav Rattan, and Martin Grohe. Weisfeiler and leman go neural: Higher-order graph neural networks. In *Proceedings of the AAAI Conference on Artificial Intelligence*, volume 33, pages 4602–4609, 2019.
- Jørgen Bang-Jensen and Gregory Z Gutin. *Digraphs: theory, algorithms and applications*. Springer Science & Business Media, 2008.
- Thomas N Kipf and Max Welling. Variational graph auto-encoders. *arXiv preprint arXiv:1611.07308*, 2016b.
- Yi Ma, Jianye Hao, Yaodong Yang, Han Li, Junqi Jin, and Guangyong Chen. Spectral-based graph convolutional network for directed graphs. *arXiv preprint arXiv:1907.08990*, 2019.
- Zekun Tong, Yuxuan Liang, Changsheng Sun, Xinke Li, David Rosenblum, and Andrew Lim. Digraph inception convolutional networks. *Advances in Neural Information Processing Systems*, 33, 2020a.
- Chensheng Li, Xiaowei Qin, Xiaodong Xu, Dujia Yang, and Guo Wei. Scalable graph convolutional networks with fast localized spectral filter for directed graphs. *IEEE Access*, 8:105634–105644, 2020.
- Federico Monti, Karl Otness, and Michael M Bronstein. Motifnet: a motif-based graph convolutional network for directed graphs. In *2018 IEEE Data Science Workshop (DSW)*, pages 225–228. IEEE, 2018.
- Michael Kampffmeyer, Yinbo Chen, Xiaodan Liang, Hao Wang, Yujia Zhang, and Eric P Xing. Rethinking knowledge graph propagation for zero-shot learning. In *Proceedings of the IEEE/CVF Conference on Computer Vision and Pattern Recognition*, pages 11487–11496, 2019.
- Michael Schlichtkrull, Thomas N Kipf, Peter Bloem, Rianne Van Den Berg, Ivan Titov, and Max Welling. Modeling relational data with graph convolutional networks. In *European semantic web conference*, pages 593–607. Springer, 2018.
- Zekun Tong, Yuxuan Liang, Changsheng Sun, David S Rosenblum, and Andrew Lim. Directed graph convolutional network. *arXiv preprint arXiv:2004.13970*, 2020b.
- Chang Zhou, Yuqiong Liu, Xiaofei Liu, Zhongyi Liu, and Jun Gao. Scalable graph embedding for asymmetric proximity. In *Proceedings of the AAAI Conference on Artificial Intelligence*, volume 31, 2017.
- Guillaume Salha, Stratis Limnios, Romain Hennequin, Viet-Anh Tran, and Michalis Vazirgiannis. Gravity-inspired graph autoencoders for directed link prediction. In *Proceedings of the 28th ACM International Conference on Information and Knowledge Management*, pages 589–598, 2019.
- Veronika Thost and Jie Chen. Directed acyclic graph neural networks. *arXiv preprint arXiv:2101.07965*, 2021.

- Guillaume Jaume, An-phi Nguyen, María Rodríguez Martínez, Jean-Philippe Thiran, and Maria Gabrani. edgnn: a simple and powerful gnn for directed labeled graphs. *arXiv preprint arXiv:1904.08745*, 2019.
- Francesco Orsini, Paolo Frasconi, and Luc De Raedt. Graph invariant kernels. In *Proceedings of the twenty-fourth international joint conference on artificial intelligence*, volume 2015, pages 3756–3762. IJCAI-INT JOINT CONF ARTIF INTELL, 2015.
- Martin Grohe, Kristian Kersting, Martin Mladenov, and Pascal Schweitzer. Color refinement and its applications. *Van den Broeck, G.; Kersting, K.; Natarajan, S*, page 30, 2017.
- Dengyong Zhou, Thomas Hofmann, and Bernhard Schölkopf. Semi-supervised learning on directed graphs. In *Advances in neural information processing systems*, pages 1633–1640, 2005.
- Matthias Fey and Jan E. Lenssen. Fast graph representation learning with PyTorch Geometric. In *ICLR Workshop on Representation Learning on Graphs and Manifolds*, 2019.
- Oleksandr Shchur, Maximilian Mumme, Aleksandar Bojchevski, and Stephan Günnemann. Pitfalls of graph neural network evaluation. *arXiv preprint arXiv:1811.05868*, 2018.
- Richard B. Lehoucq, Danny C. Sorensen, and Chao Yang. *ARPACK users' guide - solution of large-scale eigenvalue problems with implicitly restarted Arnoldi methods*. Software, environments, tools. SIAM, 1998. ISBN 978-0-89871-407-4.
- Nathan Halko, Per-Gunnar Martinsson, and Joel A Tropp. Finding structure with randomness: Probabilistic algorithms for constructing approximate matrix decompositions. *SIAM review*, 53(2):217–288, 2011.
- Laurens Van der Maaten and Geoffrey Hinton. Visualizing data using t-sne. *Journal of machine learning research*, 9(11), 2008.